Effects of in-plane stiffness and charge transfer on thermal expansion of monolayer transition metal dichalcogenide*

Wang Zhan-Yu(王占雨)[a)b)], Zhou Yan-Li(周艳丽)[c)], Wang Xue-Qing(王雪青)[b)], Wang Fei(王 飞)[a)b)], Sun Qiang(孙 强)[a)b)], Guo Zheng-Xiao(郭正晓)[a)b)d)], and Jia Yu(贾 瑜)[a)b)†]

[a)] International Joint Research Laboratory for Quantum Functional Materials of Henan, Zhengzhou University, Zhengzhou 450001, China
[b)] School of Physics and Engineering, Zhengzhou University, Zhengzhou 450001, China
[c)] Department of Mechanical and Electrical Engineering, Henan Industry and Trade Vocational College, Zhengzhou 451191, China
[d)] Department of Chemistry, University College London, London WC1H 0AJ, U.K.

(Received 11 July 2014; revised manuscript received 13 October 2014; published online 10 December 2014)

The temperature dependence of lattice constants is studied by using first-principles calculations to determine the effects of in-plane stiffness and charge transfer on the thermal expansions of monolayer semiconducting transition metal dichalcogenides. Unlike the corresponding bulk material, our simulations show that monolayer MX_2 (M = Mo and W; X = S, Se, and Te) exhibits a negative thermal expansion at low temperatures, induced by the bending modes. The transition from contraction to expansion at higher temperatures is observed. Interestingly, the thermal expansion can be tailored regularly by alteration of the M or X atom. Detailed analysis shows that the positive thermal expansion coefficient is determined mainly by the in-plane stiffness, which can be expressed by a simple relationship. Essentially the regularity of this change can be attributed to the difference in charge transfer between the different elements. These findings should be applicable to other two-dimensional systems.

Keywords: transition metal dichalcogenide, thermal expansion, phonon

PACS: 65.80.–g, 63.22.Np **DOI:** 10.1088/1674-1056/24/2/026501

1. Introduction

Understanding the thermal and structural properties of two-dimensional (2D) systems is one of the most important and fundamental issues in science with a wide spectrum of applications.[1] In the quasi-harmonic approximation (QHA), the thermal expansion coefficient[2] for a three-dimensional (3D) crystal is equal to $(1/BV)\sum_{q,j}\Gamma_{q,j}c_{v_{q,j}}(T)$ (where B is the bulk modulus, V is the unit cell volume, $\Gamma_{q,j}(=-\partial\ln\omega_{q,j}/\partial\ln V)$ is the Grüneisen parameter of the vibrational state with frequency $\omega_{q,j}$, and $c_{v_{q,j}}(T)$ is the specific heat). Therefore, the volumetric thermal expansion varies inversely with the bulk modulus. However, for a 2D monolayer structure, the thickness becomes ambiguous. The in-plane stiffness is regarded as a more suitable measure of the rigidity rather than the bulk modulus.[3–5] Owing to sharing the same hexagonal lattice, the monolayer semiconducting transition metal dichalcogenide (STMD) is an ideal prototype to determine the correlation between thermal expansion and in-plane stiffness.

The STMD is gaining increasing attention and offers an opportunity for fundamental and technological research in a variety of fields including catalysis, energy storage, sensing, and electronic devices such as field-effect transistors and logic circuits.[6–14] For instance, monolayer MoS_2, a prototypical example of STMD with a large intrinsic direct bandgap of $\sim$ 1.8 eV,[15] is a very desirable candidate for optoelectronics and digital electronics with thermal stability up to 1100.[9,16,17] However, the performance of the complex MX_2-based devices will change significantly due to internal stresses imposed by different expansion coefficients. Thus it is important to determine the thermal expansion coefficient as a function of temperature.[18–21] In addition, according to the ubiquitous membrane effect,[22,23] the ZA bending acoustic modes may cause negative thermal expansion in membranes or layered materials. In particular, many studies on graphene, graphite, and boron nitride have directly manifested this phenomenon.[24] Thus, the monolayer STMD is also expected to contract at some specific temperatures.

In this article, first-principles phonon calculations are used to determine how the lattice constant of monolayer MX_2 changes with the increase of temperature. Unlike the corresponding bulk material,[25] monolayer MX_2 shows a negative thermal expansion (NTE) at low temperatures. The positive linear thermal expansion coefficient of a 2D system can be written as $(1/A_0C)\sum_{q,j}\Gamma'_{q,j}c_{v_{q,j}}(T)$, where C is the in-plane stiffness, A_0 is the equilibrium area for the single layer, and $\Gamma'_{q,j}(=-\partial\ln\omega_{q,j}/\partial\ln a)$ is the mode Grüneisen parameter. Thus, the thermal expansion of a 2D system shows the in-

*Project supported by the National Natural Science Foundation of China (Grant Nos. 11274280 and 11104254) and the National Basic Research Program of China (Grant No. 2012CB921300).

†Corresponding author. E-mail: jiayu@zzu.edu.cn

© 2015 Chinese Physical Society and IOP Publishing Ltd

verse correlation with the in-plane stiffness C. Furthermore, our calculated results show that the difference in their in-plane stiffness can be attributed to the difference in charge transfer.

2. Computational details

The static lattice energy and the Hellmann–Feynman force are calculated using the density-functional theory (DFT), implemented in the Vienna *ab initio* simulation package (VASP).[26–28] The projector-augmented wave function (PAW) method[29] with the Perdew–Burke–Ernzerh[30] (PBE) of generalized gradient approximation (GGA) is adopted. A large spacing of ~ 15 Å between 2D single layers of MX_2 is taken to prevent interlayer interactions. The plane-wave energy cutoffs are 470 eV (WS_2), 400 eV (MoS_2, WSe_2, and WTe_2), and 380 eV ($MoSe_2$ and $MoTe_2$). The Brillouin-zone (BZ) is sampled by a $10\times10\times1$ Gamma centered k mesh for the primitive MX_2 unit cell. The total energy is calculated with high precision, and converges to 10^{-8} eV/atom. And the lattice constants and the atom coordinates are optimized until the interatomic force is less than 10^{-6} eV/Å.

The phonon calculations are performed by using the supercell method through the PHONOPY code,[31] and the real-space force constants of supercells are calculated by using the density-functional perturbation theory (DFPT) as implemented in VASP. In our calculations, the nonanalytic contribution to the dynamical matrix in the limit $q \to 0$ is even smaller and is neglected. Then the thermal expansion of MX_2 can be calculated by the phonon dispersions based on the QHA. Within the QHA, Helmholtz free energy $F(T,\{a_i\})$ with respect to all the geometrical degrees of freedom $\{a_i\}$ in a crystal is expressed as[32,33]

$$F(T,\{a_i\}) = E(\{a_i\}) + F_{\rm vib}(T,\{a_i\}), \tag{1}$$

where $E(\{a_i\})$ is the total energy of the solid when all atoms are fixed at their crystalline lattice sites, and the second term on the right-hand side is the vibrational contribution to the Helmholtz free energy, which can be calculated using the relationship[34]

$$F_{\rm vib}(T,\{a_i\}) = \sum_{q,j}\frac{\hbar\omega_{q,j}(\{a_i\})}{2} + k_{\rm B}T \times \sum_{q,j}\ln\left[1-\exp\left(-\frac{\hbar\omega_{q,j}(\{a_i\})}{k_{\rm B}T}\right)\right], \tag{2}$$

where $\omega_{q,j}(\{a_i\})$ indicates the dependence of the phonon frequency on the structural parameters $\{a_i\}$. For our QHA calculations, necessary routine numerical checks on the reliability of the supercell size are made and supercells containing $4\times4\times1$ primitive cells are chosen for all STMDs. Direct minimization of the free energy $F(T,\{a_i\})$ provides the corresponding equilibrium structure at temperature T and zero pressure. So their linear thermal expansions are easily obtained as a variation in the equilibrium lattice constants.

According to Grüneisen theory, the linear thermal expansion coefficient for monolayer MX_2 can be given by[24]

$$\alpha_i(T) = \frac{1}{a_0^2\dfrac{\partial^2 E}{\partial a^2}\Big|_0}\sum_{q,j}\Gamma'_{q,j}c_{\upsilon_{q,j}}(T), \tag{3}$$

where the subscript "0" indicates a quantity taken at the ground state lattice parameter. Since $c_{\upsilon_{q,j}}(T)$ is always positive, it is clear that the negative thermal expansion results only from negative values of the Grüneisen parameters for certain phonons. Note that the term $a_0^2\left(\partial^2E/\partial a^2\right)\big|_0$ in Eq. (3) is equal to $9V_0B_0$ for 3D isotropic crystalline solid.

3. Results and discussion

3.1. In-plane stiffness and charge transfer

The crystal structure of 2H–MX_2 belongs to the D_{6h}^4 point group (space group $P6_3/mmc$), and the unit cell consists of six atoms.[35] In contrast, monolayer MX_2 belongs to the space group $P6m2$. The M and X atoms form a hexagonal lattice with trigonal prismatic coordination as depicted in Fig. 1. The calculated structural parameters are listed in Table 1. The data show that the lattice constants of MX_2 monolayers of the same X atoms, which are nearly identical, and other lattice parameters, such as the bond angles, change slightly. For MoX_2 or WX_2, the structural parameters including lattice constants increase significantly with increasing the X atomic radius. Experimental data of the lattice parameters of monolayer STMD are not available yet. However, our calculated lattice constants are close to those of their bulk counterparts. For example, the optimized lattice constant of the MoS_2 is 3.19 Å, which is almost the same as the experimental value (3.16 Å)[36] of 2H–MoS_2.

For the single layer MX_2, the in-plane stiffness C mentioned above can be given as[37] $1/A_0\left(\partial^2E_{\rm S}/\partial\varepsilon^2\right)$, where $E_{\rm S}$ is the strain energy calculated by subtracting the total energy at zero strain from the total energy at a given strain ($E_{\rm S} = E_\varepsilon - E_{\varepsilon=0}$), and ε is the in-plane uniaxial strain ($\varepsilon = \Delta a/a$). In Table 1, in-plane stiffness and the charge transfers of metals for these monolayer semiconductors are also presented. Using the Bader analysis,[38] the charge transfer from the metal to the chalcogen atom is obtained. For MoX_2 or WX_2, the charge transfer decreases with increasing the row number of the X atom. Generally, the higher the charge transfer, the larger the in-plane stiffness is. Thus the in-plane stiffness decreases with increasing the row number of X. Moreover, the in-plane stiffness of WX_2 is usually higher than those of MoX_2.

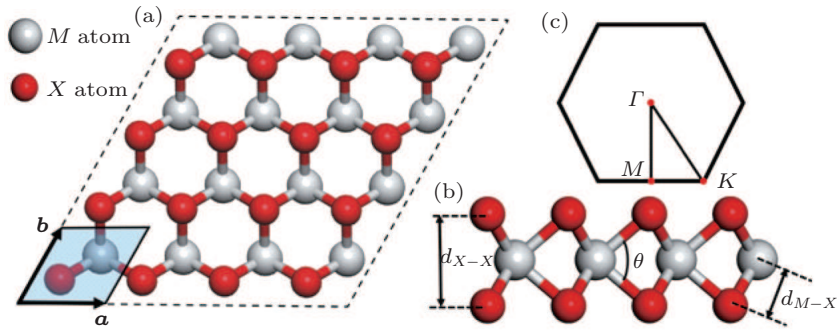


Fig. 1. (color online) (a) Top and (b) side views of the atomic structure of monolayer MX_2. The figure shows a 4×4 supercell, and the primitive unit cell with lattice vectors $\boldsymbol{a}$ and $\boldsymbol{b}$ ($|\boldsymbol{a}| = |\boldsymbol{b}|$) is highlighted by a parallelogram. The relevant internal structural parameters are also indicated. (c) Corresponding Brillouin zone with some high-symmetry points.

Table 1. Calculated values of lattice constant a, bond lengths (d_{M-X} and d_{X-X}), X–M–X bond angle θ, in-plane stiffness C, and charge transfer of metal ΔQ for monolayer STMD.

	a/Å	d_{M-X}/Å	d_{X-X}/Å	θ/(°)	C/(N/m)	ΔQ/electrons
MoS_2	3.191	2.418	3.134	80.758	168.15	1.19
$MoSe_2$	3.327	2.547	3.345	82.097	125.34	0.94
$MoTe_2$	3.557	2.737	3.620	82.792	91.38	0.59
WS_2	3.194	2.423	3.145	80.927	194.95	1.34
WSe_2	3.326	2.552	3.363	82.418	138.04	1.05
WTe_2	3.560	2.743	3.632	82.926	102.17	0.64

3.2. Phonon

Phonons play a crucial role in determining the thermodynamic properties of crystal. Before determining the thermal expansion of monolayer STMD, it is imperative to investigate their vibrational properties systematically. Since monolayer MX_2 has three atoms per primitive cell and is given by point group D_{3h}, besides three acoustic modes, six optical modes $(2E'' + 2E' + A_1' + A_2'')$ at the BZ center are therefore expected. Several studies on their vibrational properties have been reported. For example, Najmaei *et al.*[39] examined the temperature dependences of the MoS_2 vibrational modes with thickness values ranging from a single layer to a few layers. They demonstrated that thermal expansion plays a significant role in determining the temperature dependence of the out-of-plane mode A_{1g}, corresponding to the A_1' mode of the monolayer MoS_2.

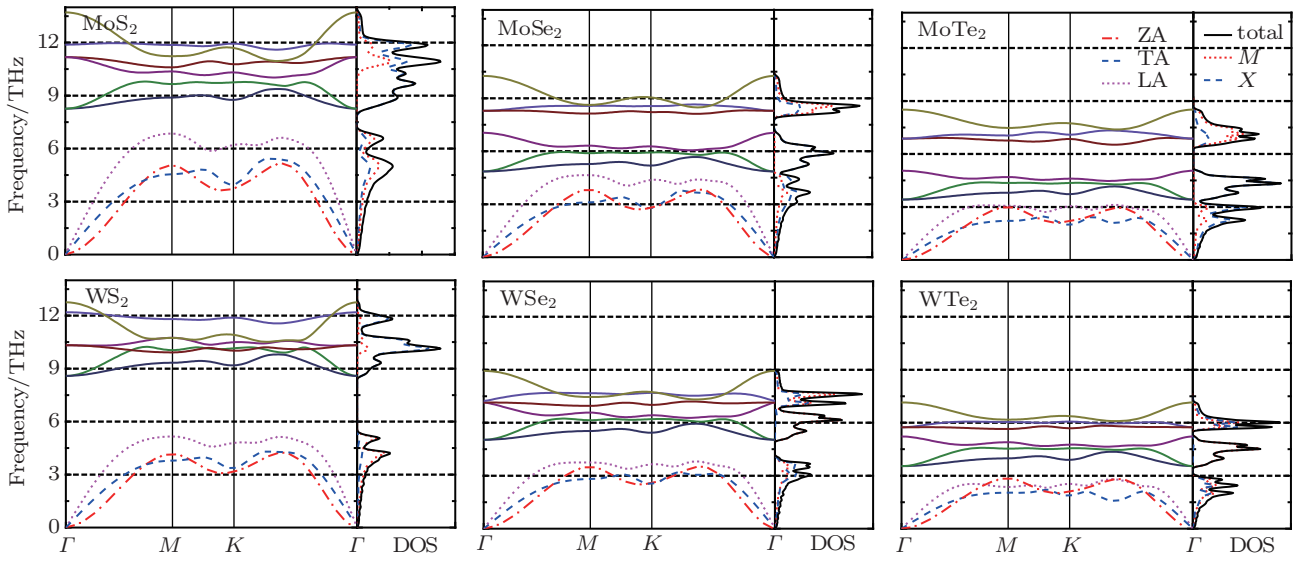


Fig. 2. (color online) *Ab initio* calculations of phonon dispersion curves along the Γ–M–K–Γ direction of the BZ, and vibrational density of states (DOS) for monolayer MX_2 at the equilibrium volume. All branches are presented with sharing the same scale of frequency. All acoustical modes (ZA, TA, and LA) as well as vibrational DOS are shown using the same graph legend.

Figure 2 shows the calculated phonon dispersion curves for monolayer MX_2 along the high-symmetry points in the first BZ. The calculated acoustical and optical branches of monolayer STMD are positive for any point in BZ, indicating that these suspended, monolayer MX_2 compounds are stable. As a characteristic feature of the phonon dispersion of layered crystals, the out-of-plane acoustical (ZA) mode of monolayer MX_2 displays a parabolic dispersion because the transverse force

decays exponentially, in contrast to the in-plane longitudinal acoustic (LA) and transverse acoustic (TA) branches showing linear dispersions near the Γ point. From Fig. 2, it is clear that the widths of the acoustical and optical branches of MoX_2 or WX_2 decrease with increasing the row number of the X atom. This is mainly because the strength of the M–X bond reduces as the mass of the X atom increases.

In order to understand clearly their vibrational properties, the frequencies and the corresponding atomic displacements of the optical modes (E'', E', A_1', and A_2'') at the Γ point are plotted in Fig. 3. For E'' and A_1' modes, which are associated with the motions of chalcogen atoms, the vibrational frequencies are determined just by the strength of the M–X bonding. So these modes for WX_2 are shifted toward higher frequencies with respect to the MoX_2 frequencies. However, the opposite results are obtained for E' and A_2'' modes involving the vibrations of both metal and chalcogen atoms, as a result of the heavy metal atom in WX_2. Additionally, in Fig. 3, the available experimental data[35,40,41] are also presented for comparison. Considering the fact that PBE tends to underestimate the phonon frequencies, the experimental data are well reproduced by our calculations.

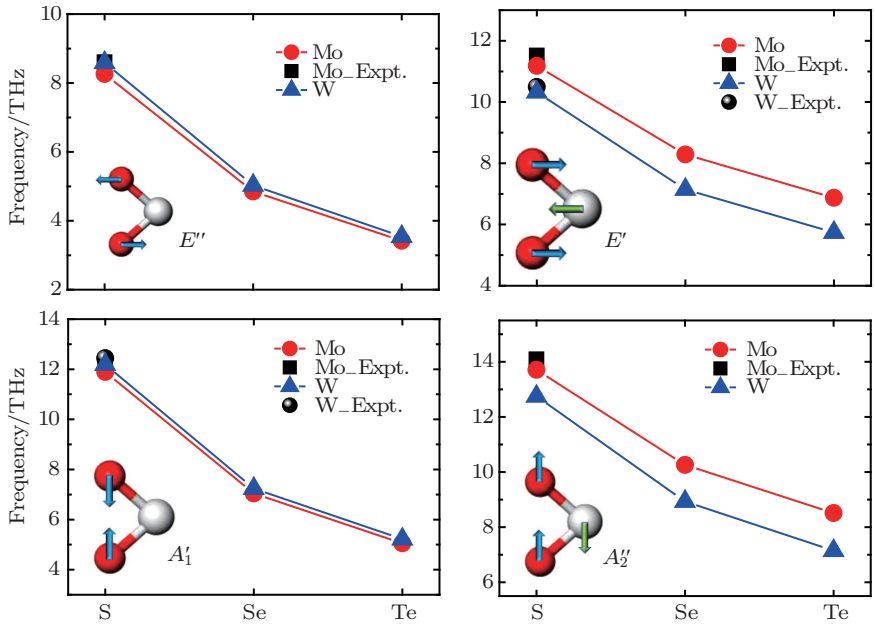


Fig. 3. (color online) Frequencies of the optical modes at Γ-point for monolayer STMD. Experimental data are cited from Refs. [35], [40], and [41]. The insets show the symmetry representations and the corresponding atomic displacements.

3.3. Thermal expansion

To understand further the contributions of the various modes to thermal expansion, the Grüneisen parameters corresponding to different phonon modes for the monolayer MX_2 and those in some high-symmetry directions are shown in Fig. 4. A generalized Grüneisen parameter can be given by[42] $\Gamma'_{q,j} = -1/\omega_{0,q,j}(\partial\omega_{q,j}/\partial\varepsilon)$, which expresses the Grüneisen parameter as a response of the frequency to thermal strain. From the figure, the Grüneisen parameters for the high-frequency optical branches show very little change in a range between 0 to $\sim$ 1. For MoS_2 and WS_2, there are quite strong inter-atomic forces, as revealed by the in-plane stiffness. So their acoustical branches are not strongly affected by the thermal strain, that is, the responses (Grüneisen parameters) do not change much. However, for the other MoX_2 or WX_2 exhibiting relatively small in-plane stiffness, the Grüneisen parameters for these branches are more scattered as the chalcogen atoms go from Se to Te. Interestingly, for $MoTe_2$ and WTe_2, some parameters for LA and TA modes ultimately become negative.

In contrast to graphene,[24] in all the monolayer STMDs only a few Grüneisen parameters for the out-of-plane ZA modes are negative, and most are positive. Based on the Bader analysis shown in Table 1, charge transfer gives rise to an excess charge around chalcogen atoms. Consequently, monolayer MX_2 can be viewed as a positively charged metal plane sandwiched between two negatively charged planes of chalcogen atoms. Intuitively, this special sandwich structure forms a strong intra-layer interaction, thus will suppress the so-called membrane effect that can be envisioned as bending induced contraction of the layer. So it is not surprising that the monolayer MX_2 crystals only have a few negative Grüneisen parameters for the ZA modes. Also, it is not difficult to speculate that their thermal expansion coefficients will be negative at extremely low temperatures.

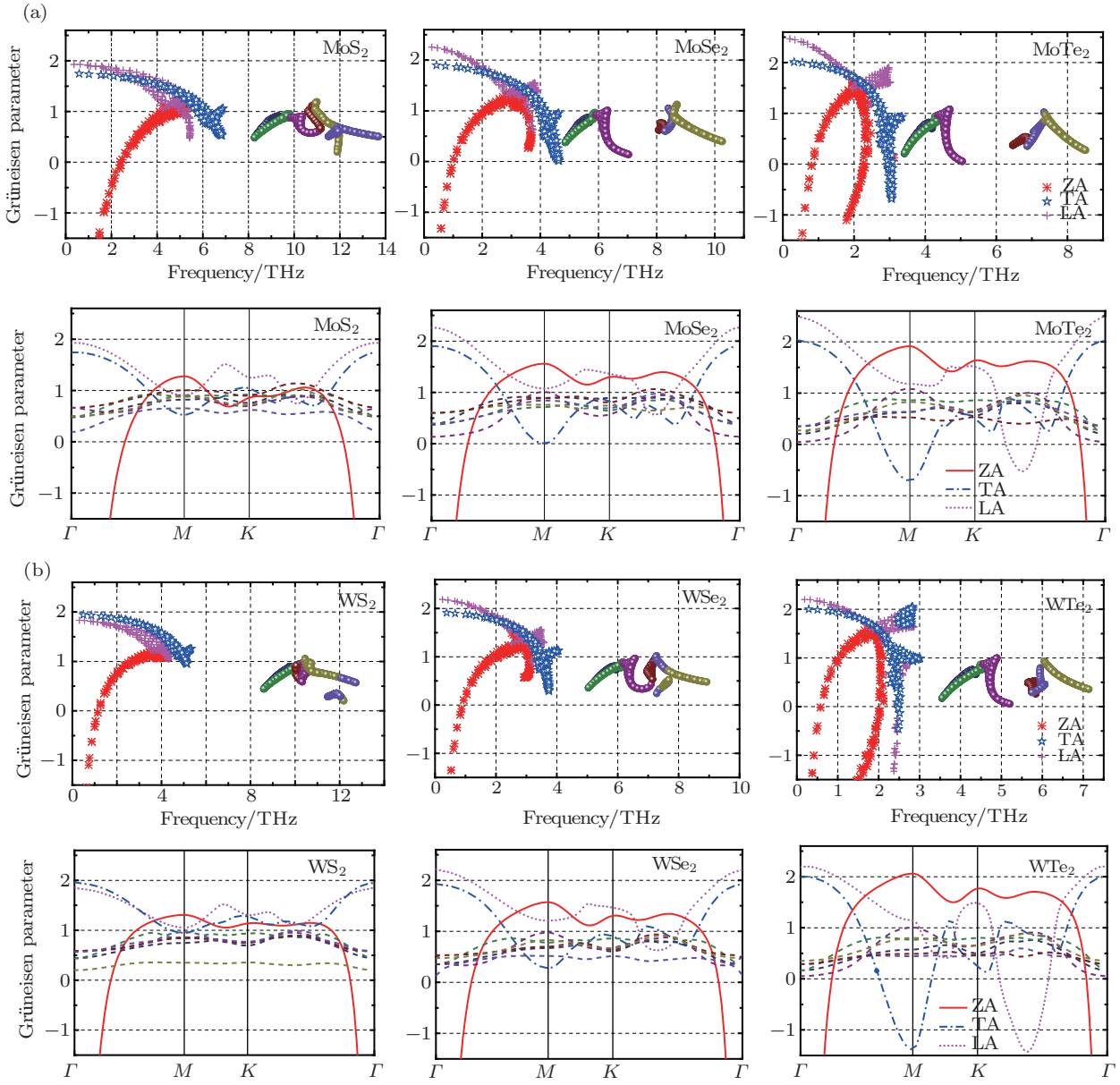


Fig. 4. (color online) Calculated mode Grüneisen parameters for monolayers of (a) MoX_2 and (b) WX_2. In panels (a) and (b), the mode Grüneisen parameters as a function of frequency are presented in the first row, and these values along high-symmetry directions are in the second row. All the mode Grüneisen parameters of the optical phonons are shown without graph legend.

It is indeed shown in Fig. 5 that the linear thermal expansion coefficients for monolayer STMDs exhibit the expected small thermal contractions only in a low-temperature region. The data for MoS_2 and $MoSe_2$ obtained by our implementation are in excellent agreement with the reported results.[43] For MoS_2, showing the maximum thermal contraction among these compounds, the lattice length decreases gradually as the temperature increases from 0 to 31 K. The minimum value of the linear thermal expansion coefficient is -2.0×10^{-7} K^{-1} and occurs at $T = 15$ K. In this low temperature region the bending modes, which possess very low energy, are responsible for the thermal contraction. At $T = 31$ K, the lattice length is smallest, and then the thermal contraction turns to an expansion. From 31 K to $\sim$ 300 K, where more high-energy optical modes are excited, $\alpha_i(T)$ increases rapidly with increasing the temperature. Above 300 K this value begins to increase very slowly. For $MoTe_2$ and WTe_2, their thermal contractions are relatively small and occur only at $T < 9$ K and $T < 6$ K respectively. Moreover, the monolayer STMDs are important in illustrating the general thermal expansion phenomenon in 2D materials.

When the monolayer MX_2 is under an in-plane uniaxial strain arising from thermalization, a useful equation can be expressed as

$$a_0^2 \frac{\partial^2 E}{\partial a^2}\bigg|_0 = \frac{\partial^2 E_S}{\partial \varepsilon^2} = A_0 C. \tag{4}$$

According to Eq. (3), the linear thermal expansion coefficient

in terms of the in-plane stiffness C can be written as

$$\alpha_i(T) = \frac{1}{A_0 C} \sum_{q,j} \Gamma'_{q,j} c_{v_{q,j}}(T). \quad (5)$$

Therefore, $\alpha_i(T)$ varies inversely with respect to the in-plane stiffness C for monolayer MX_2. However, the negative thermal expansion of monolayer MX_2 is the result of the bending effect, and is hardly affected by the in-plane stiffness. So equation (5) is not applicable to the negative thermal expansion of monolayer MX_2.

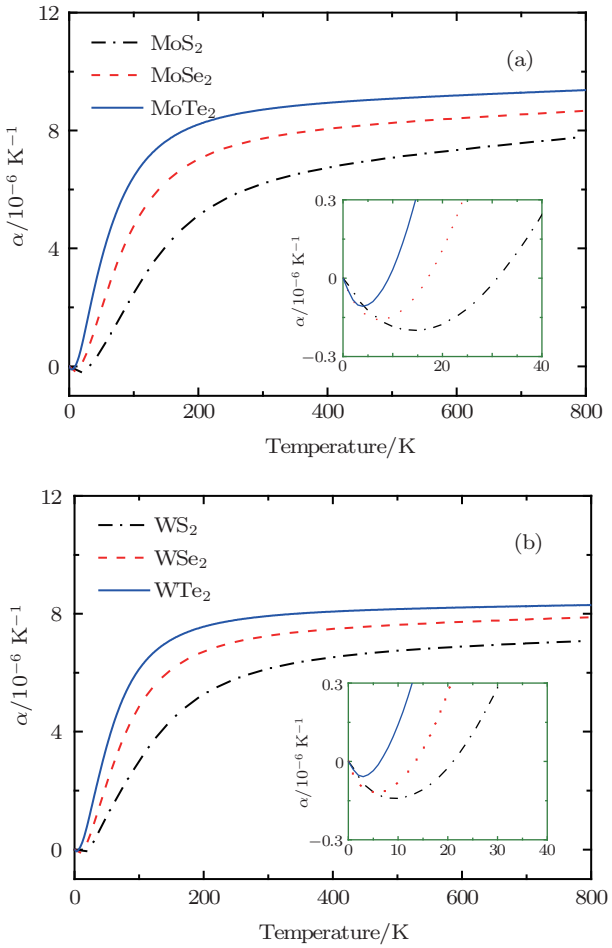


Fig. 5. (color online) Calculated thermal expansions in monolayers of (a) MoX_2, and (b) WX_2.

Figure 6 shows the variations of charge transfer of metal, in-plane stiffness, and linear thermal expansion coefficients at 300 K for the monolayer STMDs. For MoX_2 and WX_2, as the chalcogen atoms go from S, Se, to Te, the trends of variation of their thermal expansions are contrary to those of the in-plane stiffness and charge transfers. Moreover, the linear thermal expansion coefficient of WX_2 is a little smaller than that of MoX_2, because the former possesses a larger in-plane stiffness. Clearly these calculated results well validate Eq. (5) and the relevant discussion mentioned above. In summary, the effects of in-plane stiffness and charge transfers on the thermal expansions of the monolayer STMDs are further clarified. The differences in their positive thermal expansions are determined mainly by the in-plane stiffness. Indeed, these differences can be attributed to the fundamental difference in the level of charge transfer from M to the X atom. In the case of negative thermal expansion, the discrepancies may be due to the difference in bending stiffness among the monolayer STMDs.

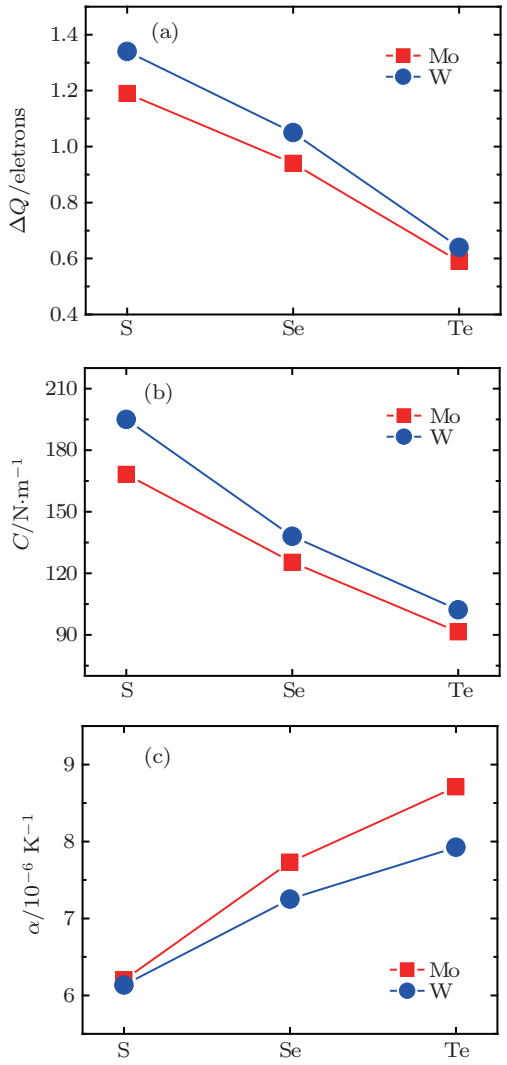


Fig. 6. (color online) Variations of (a) charge transfers of metal ΔQ, (b) in-plane stiffness C, and (c) linear thermal expansion coefficient α at 300 K for monolayer STMDs.

4. Conclusions

First-principles phonon calculations clearly show the interrelationships among the thermal expansions, in-plane stiffness, and charge transfers in monolayer STMDs. The thermal contraction of monolayer MX_2 is very small and appears only at extremely low temperatures. The mode Grüneisen parameters show that the ZA bending acoustic modes are responsible for the contraction, in a direct manifestation of the membrane effect. Their positive thermal expansion coefficients follow the order of MoX_2 > WX_2 and MS_2 < MSe_2 < MTe_2. These

changes can be well explained by the equation

$$\alpha_i(T) = \frac{1}{A_0 C} \sum_j \Gamma_j' c_{\upsilon_j}(T).$$

That is, $\alpha_i(T)$ varies inversely with the in-plane stiffness C. Essentially, the difference in their positive thermal expansions can be attributed to the fundamental differences in charge transfer from M to the X atom. The observation is beneficial to the practical applications of STMDs and the understanding of the thermal stability of other 2D systems.

Acknowledgment

One of the authors (Z. Y. Wang) is grateful to professor Wang Song-You in Fudan University for their helpful discussion. The calculations were performed on the High Performance Clusters of Zhengzhou University.

References

[1] Zakharchenko K V, Katsnelson M I and Fasolino A 2009 *Phys. Rev. Lett.* **102** 046808
[2] Li Z L and Cheng X L 2014 *Chin. Phys. B* **23** 046201
[3] Reddy C D, Rajendran S and Liew K M 2006 *Nanotechnology* **17** 864
[4] Topsakal M, Cahangirov S and Ciraci S 2010 *Appl. Phys. Lett.* **96** 091912
[5] Şahin H, Topsakal M and Ciraci S 2011 *Phys. Rev. B* **83** 115432
[6] Coleman J N, Lotya M, O'Neill A, *et al*. 2011 *Science* **331** 568
[7] Chhowalla M, Shin H S, Eda G, Li L J, Loh K P and Zhang H 2013 *Nat. Chem.* **5** 263
[8] Wang Q H, Kalantar-Zadeh K, Kis A, Coleman J N and Strano M S 2012 *Nat. Nanotechnol.* **7** 699
[9] Radisavljevic B, Radenovic A, Brivio J, Giacometti V and Kis A 2011 *Nat. Nanotechnol.* **6** 147
[10] Benameur M M, Radisavljevic B, Héron J S, Sahoo S, Berger H and Kis A 2011 *Nanotechnology* **22** 125706
[11] Zhao W, Ghorannevis Z, Chu L, Toh M, Kloc C, Tan P H and Eda G 2013 *ACS Nano* **7** 791
[12] Tao P, Guo H H, Yang T and Zhang Z D 2014 *Chin. Phys. B* **23** 106801
[13] Tongay S, Zhou J, Ataca C, Lo K, Matthews T S, Li J, Grossman J C and Wu J 2012 *Nano Lett.* **12** 5576
[14] Miró P, Ghorbani-Asl M and Heine T 2013 *Adv. Mater.* **25** 5473
[15] Mak K F, Lee C, Hone J, Shan J and Heinz T F 2010 *Phys. Rev. Lett.* **105** 136805
[16] Lopez-Sanchez O, Lembke D, Kayci M, Radenovic A and Kis A 2013 *Nat. Nanotechnol.* **8** 497
[17] Shi Y, Zhou W, Lu A Y, Fang W, Lee Y H, Hsu A L, Kim S M, Kim K K, Yang H Y, Li L J, Idrobo J C and Kong J 2012 *Nano Lett.* **12** 2784
[18] Kwon Y K, Berber S and Tománek D 2004 *Phys. Rev. Lett.* **92** 015901
[19] Yoon D, Son Y W and Cheong H 2011 *Nano Lett.* **11** 3227
[20] Singh V, Sengupta S, Solanki H S, Dhall R, Allain A, Dhara S, Pant P and Deshmukh M M 2010 *Nanotechnology* **21** 165204
[21] Jiang J W, Wang J S and Li B 2009 *Phys. Rev. B* **80** 205429
[22] Belenkii G L, Abdullayeva S G, Solodukhin A V and Suleymanov R A 1982 *Solid State Commun.* **44** 1613
[23] Abdullaev N A, Suleimanov R A, Aldzhanov M A and Alieva L N 2002 *Phys. Solid State* **44** 1859
[24] Mounet N and Marzari N 2005 *Phys. Rev. B* **71** 205214
[25] Murray R and Evans B 1979 *J. Appl. Crystallogr.* **12** 312
[26] Kresse G and Furthmiiller J 1996 *Comput. Mater. Sci.* **6** 15
[27] Kresse G and Furthmüller J 1996 *Phys. Rev. B* **54** 11169
[28] Kresse G and Joubert D 1999 *Phys. Rev. B* **59** 1758
[29] Blöchl P E 1994 *Phys. Rev. B* **50** 17953
[30] Perdew J P, Burke K and Ernzerhof M 1996 *Phys. Rev. Lett.* **77** 3865
[31] Togo A, Oba F and Tanaka I 2008 *Phys. Rev. B* **78** 134106
[32] Ren D H and Cheng X L 2012 *Chin. Phys. B* **21** 127103
[33] Wang Z, Wang F, Wang L, Jia Y and Sun Q 2013 *J. Appl. Phys.* **114** 063508
[34] Souvatzis P and Eriksson O 2008 *Phys. Rev. B* **77** 024110
[35] Matte H S S R, Gomathi A, Manna A K, Late D J, Datta R, Pati S K and Rao C N R 2010 *Angew. Chemie* **122** 4153
[36] Bollinger M V, Jacobsen K W and Nørskov J K 2003 *Phys. Rev. B* **67** 085410
[37] Ataca C, Şahin H, Aktürk E and Ciraci S 2011 *J. Phys. Chem. C* **115** 3934
[38] Henkelman G, Arnaldsson A and Jónsson H 2006 *Comput. Mater. Sci.* **36** 354
[39] Najmaei S, Ajayan P M and Lou J 2013 *Nanoscale* **5** 9758
[40] Lee C, Yan H, Brus L E, Heinz T F, Hone J and Ryu S 2010 *ACS Nano* **4** 2695
[41] Rice C, Young R J, Zan R, Bangert U, Wolverson D, Georgiou T, Jalil R, and Novoselov K S 2013 *Phys. Rev. B* **87** 081307
[42] Schelling P K and Keblinski P 2003 *Phys. Rev. B* **68** 035425
[43] Sevik C 2014 *Phys. Rev. B* **89** 035422